A Hybrid Cosine Inverse Lomax-G Family of Distributions with Applications in Medical and Engineering Data

S. O. Bashiru[1*], A. M. Isa[2], A. A. Khalaf[3,4], M. A. Khaleel[4], K. C. Arum[5] and C. L. Anioke[6]

[1]Department of Mathematics and Statistics, Confluence University of Science and Technology, Osara, Kogi State, Nigeria.
[2]Department of Mathematics and Computer Science, Borno State University, Maiduguri, Nigeria
[3]Diyala Education Directorate, Diyala, Iraq.
[4] Department of Mathematics, College of Computer Science and Mathematics, Tikrit University, Tikrit, Iraq.
[5]Department of Statistics, University of Nigeria, Nsukka.
[6]Department of Electronic Engineering, University of Nigeria, Nsukka.

ABSTRACT: Statistical distributions are essential for modelling real-world phenomena in fields such as medicine, environmental science, and engineering. However, classical distributions often fail to capture complex data features like skewness and heavy tails. This study introduces a novel hybrid family of distributions, the cosine inverse Lomax (CIL)-G family, by merging the cosine-G and inverse Lomax-G families. The proposed family demonstrates enhanced flexibility and includes sub models applicable across diverse fields. Key statistical properties, including moments, entropy measures, and the quantile function, are derived. Parameter estimation is conducted using maximum likelihood, least squares, and weighted least squares techniques. Monte Carlo simulations are employed to examine the behaviour of the estimators for a specific model, the CIL-exponentiated Weibull (CILEW). The simulation results indicate that as the sample size increases, the bias and root mean squared error of the estimators decrease, demonstrating the consistency of the estimation techniques. The CILEW model is applied to three real-world datasets: (1) 40 turbocharger failure times from engineering, (2) 20 pain relief durations from medical data, and (3) 35 growth hormone treatment times from medical data. Performance is assessed using goodness-of-fit metrics such as the Akaike information criterion (AIC), Bayesian information criterion (BIC), and Kolmogorov-Smirnov (KS) tests. The CILEW model outperforms competing models, by achieving the lowest AIC values of 171.62, 41.096, 165.44 and BIC values of 180.07, 46.074, 173.22 across the three datasets, along with the highest KS p-values of 0.8786, 0.9680, 0.9640, respectively. The proposed family provides a versatile framework for modelling complex datasets, making it a valuable tool for reliability engineering, healthcare analytics, and predictive modelling applications.

KEYWORDS: Cosine-G family, Inverse Lomax-G family, Moments, quantile function, and Monte Carlo simulation.

[Received Jul. 12, 2024; Revised Mar. 5, 2025; Accepted Mar 8, 2025] Print ISSN: 0189-9546 | Online ISSN: 2437-2110

I. INTRODUCTION

The study of statistical distributions and their features is crucial for accurately describing and predicting real-world phenomena across a variety of fields. In medicine, probability distributions are used to model patient responses to treatments, understand disease progression, and predict outcomes such as infection and mortality rates. Similarly, in engineering, reliability analysis relies on probability distributions to assess the lifespan of materials, products, and systems, accounting for the likelihood of failure or malfunction under various conditions. In environmental science, statistical distributions are used to model climate data, predict weather patterns, and assess environmental risks, such as extreme weather events or pollution levels. In finance, these distributions are indispensable for modelling stock returns, predicting market behaviour, and assessing risk.

However, in many of these fields, the data do not follow a normal distribution and often exhibit complex features such as skewness, kurtosis, and heavy tails. For instance, medical datasets related to COVID-19, pain relief, and growth hormone treatments frequently display skewed distributions, where the data may show a monotonically increasing or decreasing hazard pattern. Classical distributions, while foundational in statistics, often fail to capture the complexity of these datasets. This limitation has led to the development of new families of distributions, called generators, which modify classical distributions for a better fit. These distribution families enhance the flexibility of classical distributions by incorporating additional parameters such as scale, shape, or location.

Several notable distribution families have been developed in recent years, including the Topp-Leone G family introduced by Al-Shomrani et al. (2016), the Topp-Leone odd log-logistic family proposed by Brito et al. (2017), the Type II half logistic family by Soliman et al. (2017), the Marshall-Olkin generalized-G family by Yousof et al. (2018), the generalized odd gamma-G family presented by Hosseini et al. (2018), the weighted Weibull-G family of distributions by Hassan et al. (2022), the tangent Topp-Leone family studied by Nanga et al. (2022), the type I half logistic-Topp-Leone-G distribution family by Adepoju et al. (2023), the sine type II Topp-Leone

*Corresponding author: bash0140@gmail.com
doi: http://dx.doi.org/10.4314/njtd.v22i1.2734

G family defined by Isa *et al* (2023), the new hyperbolic sine-generator formulated by Ahmad *et al.* (2023), the Topp-Leone Cauchy family introduced by Atchadé *et al.* (2023), the new sine family of generalized distributions by Benchiha *et al.* (2023), the exponentiated cosine Topp-Leone family by Osi *et al.* (2024) and the secant Kumaraswamy family developed by Nanga *et al.* (2024).

Despite these advances, the demand for diverse distribution families continues because no single model can universally fit all data types. There remains a pressing need to develop more robust families of distributions to enhance our existing knowledge base and provide greater flexibility in modelling data with diverse and complex characteristics.

In response to this need, this study aims to introduce a novel hybrid family of distributions, called the cosine inverse Lomax (CIL) generated family. This family is designed to increase the flexibility of classical distributions. The CIL family is created by combining two distinct generators: the cosine family of distributions (Souza, 2015) and the inverse Lomax generator (Falgore and Doguwa, 2020). These generators were selected for their unique properties. The cosine family enhances the flexibility of classical distributions through cosine function transformations, while the inverse Lomax generator, which incorporates scale and shape parameters, induces skewness into classical distributions, further enhancing their adaptability. By integrating these two generators, the resulting hybrid family inherits the beneficial properties of both generators. Notably, this integration has not been explored in previous research.

This study is motivated by the limitations of classical distributions in modelling complex datasets, particularly those exhibiting skewness or heavy tails, which are common in medical and other diverse fields. Classical distributions struggle to capture the intricate patterns in real-world data due to their rigid shapes and assumptions. By developing the CIL family, this research aims to address these limitations and provide a more versatile tool for fitting and understanding complex datasets. This study effectively fills a gap in the literature, as it provides a versatile tool for modelling complex data patterns that have not been well addressed by previous distribution families.

II. METHODOLOGY

A. *The Proposed Cosine Inverse Lomax G Family of Distribution*

The proposed cosine inverse Lomax G (CIL-G) family of distributions is derived by combining the cosine G family of distributions (Souza, 2015) with the inverse Lomax G family of distributions (Falgore and Doguwa, 2020). The methodology involves the following steps:

1. Baseline Distribution:

The Inverse Lomax G family serves as the baseline distribution. Its cumulative distribution function (CDF) $R(x)$ and probability distribution function (PDF) $R(x)$ are given by:

$$R(x) = \left(1 + \frac{\beta\bar{G}(x)}{G(x)}\right)^{-\alpha} \tag{1}$$

$$r(x) = \frac{\alpha\,\beta\,g(x)}{[G(x)]^2}\left(1 + \frac{\beta\bar{G}(x)}{G(x)}\right)^{-(\alpha+1)} \quad \alpha,\beta,x > 0 \tag{2}$$

where α is the scale parameter and β is the shape parameter. $g(x)$ is the PDF of a baseline distribution, $G(x)$ is PDF of a baseline distribution and $\bar{G}(x)$ is the survival function of a baseline distribution.

2. Cosine Transformation:

The CDF of the Cosine G family is defined as:

$$F(x) = 1 - \cos\left\{\frac{\pi}{2}R(x)\right\} \tag{3}$$

The corresponding PDF is given as:

$$f(x) = \frac{\pi}{2}r(x)\sin\left\{\frac{\pi}{2}R(x)\right\} \tag{4}$$

where $r(x)$ and $R(x)$ are the PDF and CDF of the baseline distribution, respectively.

3. Derivation of the CIL-G Family:

To derive the CDF of the proposed Cosine Inverse Lomax G (CIL-G) family, substitute the CDF of the Inverse Lomax G family (Equation 1) into the Cosine G family (Equation 3). This yield:

$$F(x) = 1 - \cos\left\{\frac{\pi}{2}\left(1 + \frac{\beta\bar{G}(x)}{G(x;\xi)}\right)^{-\alpha}\right\} \tag{5}$$

The corresponding PDF of the CIL-G family is obtained by substituting $R(x)$ and $r(x)$ from the Inverse Lomax G family into the PDF of the Cosine G family (Equation 4). This results in:

$$f(x) = \frac{\pi}{2}\frac{\alpha\,\beta\,g(x;\xi)}{[G(x;\xi)]^2}\left(1 + \frac{\beta\bar{G}(x;\xi)}{G(x;\xi)}\right)^{-(\alpha+1)} \times \sin\left\{\frac{\pi}{2}\left(1 + \frac{\beta\bar{G}(x;\xi)}{G(x;\xi)}\right)^{-\alpha}\right\}, \quad \alpha,\beta,x > 0 \tag{6}$$

where ξ is the vector of parameters of the baseline distribution, $G(x;\xi)$ is the CDF of the baseline distribution with parameter vector ξ, $\bar{G}(x;\xi) = 1 - G(x;\xi)$ is the survival function of the baseline distribution, and $g(x;\xi)$ is the PDF of the baseline distribution with parameter vector ξ.

1). *Validity Proof of the CIL family of distributions*

For a PDF to represent a valid distribution, the following conditions must hold:

$$\int_{-\infty}^{\infty} f(x) = 1 \tag{7}$$

Using the PDF of the CIL family given in Equation (6), we verify this condition:

$$\int_0^{\infty}\frac{\pi\,\alpha\,\beta\,g(x;\xi)}{2\,[G(x;\xi)]^2}\left(1 + \frac{\beta\bar{G}(x;\xi)}{G(x;\xi)}\right)^{-(\alpha+1)}\sin\left\{\frac{\pi}{2}\left(1 + \frac{\beta\bar{G}(x)}{G(x;\xi)}\right)^{-\alpha}\right\}dx \tag{8}$$

$$\text{Let } p = \frac{\pi}{2}\left(1 + \frac{\beta\bar{G}(x)}{G(x;\xi)}\right)^{-\alpha} \tag{9}$$

where,

As $x \to 0$, $p \to 0$

As $x \to \infty$, $p \to \frac{\pi}{2}$

Next, we differentiate p with respect to x:

$$\frac{dp}{dx} = \frac{\pi}{2}\frac{\alpha\,\beta\,g(x;\xi)}{[G(x;\xi)]^2}\left(1 + \frac{\beta\bar{G}(x;\xi)}{G(x;\xi)}\right)^{-(\alpha+1)} \tag{10}$$

Thus, we can express dx in terms of dp:

$$dx = \frac{dp}{\frac{\pi\alpha\,\beta\,g(x;\xi)}{2\,[G(x;\xi)]^2}\left(1+\frac{\beta\bar{G}(x;\xi)}{G(x;\xi)}\right)^{-(\alpha+1)}} \quad (11)$$

substituting this into the original integral, we get:

$$\int_0^{\frac{\pi}{2}} \frac{\pi}{2}\frac{\alpha\,\beta\,g(x;\xi)}{[G(x;\xi)]^2}\left(1+\frac{\beta\bar{G}(x;\xi)}{G(x;\xi)}\right)^{-(\alpha+1)} \times \sin(p)\frac{dp}{\frac{\pi\alpha\,\beta\,g(x;\xi)}{2\,[G(x;\xi)]^2}\left(1+\frac{\beta\bar{G}(x;\xi)}{G(x;\xi)}\right)^{-(\alpha+1)}} \quad (12)$$

solving this integral:

$$\int_0^{\frac{\pi}{2}} sin(p)dp = -[cos(p)]_0^{\frac{\pi}{2}} = -\left[cos\left(\frac{\pi}{2}\right) - cos(0)\right] = 1 \quad (13)$$

Thus, the integral evaluates to 1, confirming that the PDF is valid.

After determining the CDF and PDF of the CIL-G family, the following functions of the proposed family are provided: the survival function S(x), hazard function h(x), reverse hazard function r(x), and cumulative hazard function R(x).

$$S(x) = 1 - F(x) = \cos\left\{\frac{\pi}{2}\left(1+\frac{\beta\bar{G}(x)}{G(x;\xi)}\right)^{-\alpha}\right\} \quad (14)$$

$$h(x) = \frac{f(x;\xi)}{S(x;\xi)} = \frac{\pi}{2}\frac{\alpha\,\beta\,g(x;\xi)}{[G(x;\xi)]^2}\left(1+\frac{\beta\bar{G}(x;\xi)}{G(x;\xi)}\right)^{-(\alpha+1)} \times \tan\left\{\frac{\pi}{2}\left(1+\frac{\beta\bar{G}(x;\xi)}{G(x;\xi)}\right)^{-\alpha}\right\} \quad (15)$$

$$r(x) = \frac{f(x;\xi)}{F(x;\xi)} = \frac{\frac{\pi\alpha\,\beta\,g(x;\xi)}{2\,[G(x;\xi)]^2}\left(1+\frac{\beta\bar{G}(x;\xi)}{G(x;\xi)}\right)^{-(\alpha+1)}\sin\left\{\frac{\pi}{2}\left(1+\frac{\beta\bar{G}(x;\xi)}{G(x);\xi}\right)^{-\alpha}\right\}}{1-\cos\left\{\frac{\pi}{2}\left(1+\frac{\beta\bar{G}(x;\xi)}{G(x;\xi)}\right)^{-\alpha}\right\}} \quad (16)$$

$$R(x) = -\ln\{S(x)\} = -\ln\left\{\cos\left[\frac{\pi}{2}\left(1+\frac{\beta\bar{G}(x;\xi)}{G(x;\xi)}\right)^{-\alpha}\right]\right\} \quad (17)$$

These functions are commonly utilized to elucidate a probability distribution's characteristics.

B. Expansion of the PDF for the CIL-G family of distributions

We describe the PDF of the CIL-G family of distributions as a series to facilitate the derivation of certain statistical features, such as moments and the moment generating function. After obtaining the PDF using Equation (6), the series representation takes the form:

$$\sin\left\{\frac{\pi}{2}\left(1+\frac{\beta\bar{G}(x;\xi)}{G(x;\xi)}\right)^{-\alpha}\right\} = \sum_{i=0}^{\infty}\frac{(-1)^i}{(2i+1)!}\frac{\pi^{2i+1}}{2^{2i+1}}\left(1+\frac{\beta\bar{G}(x;\xi)}{G(x;\xi)}\right)^{-\alpha i} \quad (18)$$

Then

$$f(x) = \sum_{i=0}^{\infty}\frac{\pi^{2i+2}\alpha\,\beta(-1)^i}{2^{2i+2}[G(x;\xi)]^2(2i+1)!}g(x;\xi)\left(1+\frac{\beta\bar{G}(x;\xi)}{G(x;\xi)}\right)^{-(\alpha i+\alpha+1)} \quad (19)$$

Using binomial expansion see Khalaf and Khaleel (2024)

$$\left(1+\frac{\beta\bar{G}(x;\xi)}{G(x;\xi)}\right)^{-(\alpha i+\alpha+1)} = \sum_{j=0}^{\infty}(-1)^j\beta^j\binom{\alpha i+\alpha+j}{j}\left(\frac{1-G(x;\xi)}{G(x;\xi)}\right)^j \quad (20)$$

Using the binomial expansion again,

$$(1-G(x;\xi))^j = \sum_{m=0}^{\infty}(-1)^m\binom{j+m-1}{m}G(x;\xi)^m \quad (21)$$

Therefore, the PDF expansion for the CIL-G family of distributions is:

$$f(x) = \sum_{i,j,m=0}^{\infty}\Phi_{i,j}\; g(x;\xi)G(x;\xi)^{m-j-2} \quad (22)$$

where $\Phi_{i,j} = \frac{(-1)^{i+j+m}\alpha\beta^{1-j}}{(2i+1)!}\frac{\pi^{2i+2}}{2^{2i+2}}\binom{\alpha i+\alpha+j}{j}\binom{j+m-1}{m}$

C. Expansion of the CDF for the CIL-G family of distributions

We describe the CDF of the generating function for the CIL-G family of distributions. Upon evaluating the CDF using Equation (5), consider the representation of the function as a series.

$$\cos\left\{\frac{\pi}{2}\left(1+\frac{\beta\bar{G}(x;\xi)}{G(x;\xi)}\right)^{-\alpha}\right\} = \sum_{k=0}^{\infty}\frac{(-1)^k}{2k!}\frac{\pi^{2i}}{2^{2i}}\left(1+\frac{\beta\bar{G}(x;\xi)}{G(x;\xi)}\right)^{-\alpha k} \quad (23)$$

Using binomial expansion

$$\left(1+\frac{\beta\bar{G}(x;\xi)}{G(x;\xi)}\right)^{-\alpha k} = \sum_{l=0}^{\infty}(-1)^l\binom{\alpha k}{l}\beta^l\left(1-G(x;\xi)\right)^l G(x;\xi)^{-l} \quad (24)$$

Using the binomial expansion employed by Khalaf *et al.* (2024) and Noor *et al.* (2023), we have

$$\left(1-G(x)\right)^l = \sum_{h=0}^{\infty}(-1)^h\binom{l}{h}G(x)^h \quad (25)$$

Therefore, the CDF expansion for the CIL-G family of distributions is:

$$F(x) = 1 - \sum_{k,l,h=0}^{\infty}\psi_{k,l,h}\,G(x)^{h-l} \quad (26)$$

where

$$\psi_{k,l,h} = \frac{\beta^l(-1)^{k+l+h}}{2k!}\frac{\pi^{2k}}{2^{2k}}\binom{\alpha k+l-1}{l}\binom{l}{h}$$

C. *Performance Evaluation*

The performance of the parameter estimation methods is assessed using bias and Root Mean Squared Error (RMSE)**.** The Equations for these metrics are as follows:

1. Bias:
$$bias(\hat{a}) = \frac{\sum_{i=1}^{N}\hat{a}_i}{N} - a \quad (27)$$
2. **Root Mean Squared Error (RMSE)**:
$$RMSE(\hat{a}) = \sqrt{\frac{\sum_{i=1}^{N}(\hat{a}_i - a)^2}{N}} \quad (28)$$

Additionally, the following information criteria and goodness-of-fit measures are used for model evaluation:

1. **Akaike Information Criterion (AIC)**:
$$AIC = -2l + 2K \quad (29)$$
2. **Consistent Akaike Information Criterion (CAIC)**:
$$CAIC = AIC + \frac{2K(K+1)}{n-K-1} \quad (30)$$
3. **Bayesian Information Criterion (BIC)**:
$$BIC = -2l + klog(n) \quad (31)$$
4. **Hannan-Quinn Information Criterion (HQIC)**:
$$HQIC = 2kln[\ln(n)] - 2l \quad (32)$$
5. **Cramér-von Mises (W)**:
$$W = \frac{1}{12n} + \sum_{i=1}^{n}\left[\frac{2i-1}{2n} - \hat{G}(x_i)\right]^2 \quad (33)$$
6. **Anderson-Darling (A)**:

$$A = -n - \frac{1}{n}\sum_{i=1}^{n} (2i-1)\left[\log \hat{G}(x_i) + \log\left(1 - \hat{G}(x_{n+1-i})\right)\right] \quad (34)$$

7. **Kolmogorov-Smirnov (KS)**:

$$KS = max\left\{\frac{i}{n} - \hat{G}(x_i), \hat{G}(x_i) - \frac{i-1}{n}\right\} \quad (35)$$

III. STATISTICAL PROPERTIES OF THE CIL-G FAMILY OF DISTRIBUTIONS

This section derives several statistical properties of the CIL-G family, including the quantile function, moments, moment-generating function, order statistics, Rényi entropy, and Tsallis entropy.

A. *Quantile Function of the CIL-G family of distributions*

The quantile function of x, denoted as $F^{-1}(x)$, is defined as the inverse function of F(x). Let x be a random variable that follows the CIL-G (x, α, β) family. The quantile function of x is defined as:

$$Q(u) = \left\{\frac{1}{\beta}\left[\left(\frac{\cos^{-1}(1-u)}{\pi/2}\right)^{\frac{1}{\alpha}} - 1\right] + 1\right\}^{-1} \quad (36)$$

B. *Moment of the CIL-G family of distributions*

The r[th] moment about the origin is defined as:

$$\mu_r = \int_{-\infty}^{\infty} x^r f(x;\xi)dx \quad (37)$$

Substituting Equation (11) into the Equation above, we have:

$$\mu_r = \sum_{i,j,m=0}^{\infty} \Phi_{i,j} \int_{-\infty}^{\infty} x^r g(x;\xi)G(x;\xi)^{m-j-2}dx \quad (38)$$

Therefore,

$$\mu_r = \sum_{i,j,m=0}^{\infty} \Phi_{i,j}\ \Omega \quad (39)$$

where

$$\Omega = \int_{-\infty}^{\infty} x^r g(x;\xi)G(x;\xi)^{m-j-2}dx$$

C. *Moment Generating Function of the CIL-G family of distributions*

The moment generating function (mgf) may be represented as;

$$M_x(t) = \int_{-\infty}^{\infty} e^{tx} f(x;\xi)dx \quad (40)$$

$$M_x(t) = \sum_{l=0}^{\infty} \frac{t^l}{l!}\int_0^{\infty} x^r f(x;\xi)dx \quad (41)$$

Substituting Equation (11) into the Equation above, we have:

$$M_x(t) = \sum_{l=0}^{\infty} \frac{t^l}{l!}\left(\sum_{i,j,m=0}^{\infty} \Phi_{i,j} \int_0^{\infty} e^{tx} g(x;\xi)G(x;\xi)^{m-j-2}dx\right) \quad (42)$$

Then

$$M_x(t) = \sum_{l=0}^{\infty} \frac{t^l}{l!}\left(\sum_{i,j,m=0}^{\infty} \Phi_{i,j}\ \Theta\right) \quad (43)$$

where

$$\Theta = \int_0^{\infty} e^{tx} g(x;\xi)G(x;\xi)^{m-j-2}dx$$

D. *Order Statistics of the CIL-G family of distributions*

Consider the order of statistics $x_{(1)}, x_{(2)}, \ldots, x_{(n)}$ of a random sample $x_1, x_2, \ldots, x_n$ drawn from a distribution with PDF and CDF. The i^{th} order statistics $x_{(i)}$ is expressed as:

$$f_{x_i}(x) = \frac{n!}{(r-1)(n-1)!}[F(x;\xi)]^{(r-1)}[1 - F(x;\xi)]^{(n-1)}f(x;\xi) \quad (44)$$

Substituting the Equations (5) and (6) into Equation (44):

$$f_{x_i}(x) = \frac{n!}{(r-1)(n-1)!}\left[1 - \cos\left\{\frac{\pi}{2}\left(1 + \frac{\beta\bar{G}(x;\xi)}{G(x;\xi)}\right)^{-\alpha}\right\}\right]^{(r-1)}\left[\cos\left\{\frac{\pi}{2}\left(1 + \frac{\beta\bar{G}(x;\xi)}{G(x;\xi)}\right)^{-\alpha}\right\}\right]^{(n-1)} \times \frac{\pi}{2}\frac{\alpha\,\beta\ g(x;\xi)}{[G(x;\xi)]^2}\left(1 + \frac{\beta\bar{G}(x;\xi)}{G(x;\xi)}\right)^{-(\alpha+1)} \sin\left\{\frac{\pi}{2}\left(1 + \frac{\beta\bar{G}(x;\xi)}{G(x;\xi)}\right)^{-\alpha}\right\} \quad (45)$$

E. *Rényi Entropy of the CIL-G family of distributions*

The Rényi entropy of a random variable x with distribution $f(x)$ of order θ, where $\theta > 0\ and\ \theta \neq 1$, is calculated as follows: Bashiru *et al.* (2024a)

$$R(\theta) = \frac{1}{1-\theta}\log\int_0^{\infty} f(x)^{\theta}dx \quad (46)$$

Substituting Equation (22) into Equation (46), we have:

$$R(\theta) = \frac{1}{1-\theta}\log\int_0^{\infty}\left(\sum_{i,j,m=0}^{\infty} \Phi_{i,j}\ g(x)G(x)^{m-j-2}\right)^{\theta}dx \quad (47)$$

F. *Tsallis Entropy of the CIL-G family of distributions*

The Tsallis entropy of a random variable x with distribution $f(x)$ of order δ, where $\delta > 0, \delta \neq 1$, then the Tsallis entropy for the CIL-G family is given as:

$$T(\delta) = \frac{1}{1-\delta}\left(1 - \int_0^{\infty} f(x)^{\delta}dx\right) \quad (48)$$

Substituting Equation (22) into Equation (48), we have:

$$T(\delta) = \frac{1}{1-\delta}\left(1 - \int_0^{\infty}\left(\sum_{i,j,m=0}^{\infty} \Phi_{i,j}\ g(x)G(x)^{m-j-2}\right)^{\delta}dx\right) \quad (49)$$

G. *Havrda and Charvat Entropy of the CIL-G family of distributions*

As a measure, the Havrda and Charvat entropy is given by:

$$HC_{\vartheta}(x) = \frac{1}{2^{1-\vartheta}-1}\left[\left(\int_0^{\infty}\left(f(x)\right)^{\vartheta}dx\right)^{\frac{1}{\vartheta}} - 1\right] \quad , \vartheta > 0, \vartheta \neq 1 \quad (50)$$

Substituting Equation (22) into Equation (50), we have:

$$HC_{\vartheta}(x) = \frac{1}{2^{1-\vartheta}-1}\left[\left(\int_0^{\infty}\left(\sum_{i,j,m=0}^{\infty} \Phi_{i,j}\ g(x)G(x)^{m-j-2}\right)^{\vartheta}dx\right)^{\frac{1}{\vartheta}} - 1\right] \quad (51)$$

IV. ESTIMATION OF PARAMETERS FOR THE CIL-G FAMILY OF DISTRIBUTIONS

This section discusses the methods used to estimate the parameters of the CIL-G family of distributions.

A. Maximum Likelihood Estimation

We derive the maximum likelihood estimators (MLEs) for the parameters of the new family of distributions, assuming

complete data. Consider a random sample, denoted as $x_1, x_2, \ldots, x_n$, drawn from the CIL-G family. This family is characterized by the parameters α, β, and ξ. Let $\varphi = (\alpha, \beta, \xi)^T$ be the parameter vector: Bashiru *et al.* (2024b)

The log-likelihood function for φ, denoted as $\ell = \ell(\varphi)$, is provided as follows:

$$\ell = n\log\left(\frac{\pi}{2}\right) + n\log\alpha + n\log\beta + \sum_{i=1}^{n}\log g(x;\xi) - 2\sum_{i=1}^{n}\log G(x;\xi) - (\alpha+1)\sum_{i=1}^{n}\left(1+\frac{\beta\bar{G}(x;\xi)}{G(x;\xi)}\right) + \sum_{i=1}^{n}\log\sin\left\{\frac{\pi}{2}\left(1+\frac{\beta\bar{G}(x;\xi)}{G(x;\xi)}\right)^{-\alpha}\right\} \quad (52)$$

Now, we need to determine the first-order conditions:

$$\frac{\partial\ell}{\partial\alpha} = \frac{n}{\alpha} - \sum_{i=1}^{n}\log\left(1+\frac{\beta\bar{G}(x;\xi)}{G(x;\xi)}\right) + \sum_{i=1}^{n}\frac{\pi}{2}\left(1+\frac{\beta\bar{G}(x;\xi)}{G(x;\xi)}\right)^{-\alpha}\log\left(1+\frac{\beta\bar{G}(x;\xi)}{G(x;\xi)}\right)\cot\left\{\frac{\pi}{2}\left(1+\frac{\beta\bar{G}(x;\xi)}{G(x;\xi)}\right)^{-\alpha}\right\} \quad (53)$$

$$\frac{\partial\ell}{\partial\beta} = \frac{n}{\beta} - (\alpha+1)\left(\frac{1-G(x;\xi)}{G(x;\xi)}\right)\left(1+\frac{\beta\bar{G}(x;\xi)}{G(x;\xi)}\right)^{-1} - \sum_{i=1}^{n}\frac{\alpha\pi}{2}\left(1+\frac{\beta\bar{G}(x;\xi)}{G(x\xi)}\right)^{-(\alpha+1)}\cot\left\{\frac{\pi}{2}\left(1+\frac{\beta\bar{G}(x;\xi)}{G(x;\xi)}\right)^{-\alpha}\right\} \quad (54)$$

$$\frac{\partial\ell}{\partial\xi} = \sum_{i=1}^{n}\frac{g'(x`;\xi)}{g(x;\xi)} - 2\sum_{i=1}^{n}\frac{g(x;\xi)}{G(x;\xi)} + (\alpha+1)\sum_{i=1}^{n}\frac{\beta g(x;\xi)}{[G(x;\xi)]^2}\left(1+\frac{\beta\bar{G}(x;\xi)}{G(x;\xi)}\right)^{-1} - \sum_{i=1}^{n}\frac{\alpha\pi}{2}\frac{\beta g(x;\xi)}{[G(x;\xi)]^2}\left(1+\frac{\beta\bar{G}(x;\xi)}{G(x;\xi)}\right)^{-(\alpha+1)}\cot\left\{\frac{\pi}{2}\left(1+\frac{\beta\bar{G}(x;\xi)}{G(x;\xi)}\right)^{-\alpha}\right\} \quad (55)$$

Since analytical solutions to the aforementioned non-linear Equations are not possible, we used R-code to do the necessary analytical calculations on the R software.

B. Least Squares Estimation (LSE)

The LSE approach is employed to estimate the parameters of the CIL-G distribution. This method minimizes the following Equation:

$$L(\alpha,\beta,\xi) = \sum_{i=1}^{n}\left(G\left(x_{i;n},\alpha,\beta,\xi\right) - \frac{i}{n+1}\right)^2 \quad (56)$$

C. Weighted Least Squares Estimation (WLSE)

The WLSE method is used to estimate the parameters of the CIL-G distribution. The goal is to minimize the following weighted sum of squares:

$$W(\alpha,\beta,\xi) = \sum_{i=1}^{n}\frac{(n+1)^2(n+2)}{i(n-i+1)}\left(G\left(x_{i;n},\alpha,\beta,\xi\right) - \frac{i}{n+1}\right)^2 \quad (57)$$

With a corresponding PDF:

$$f(x)\left(1+\frac{\beta\left(1-\left(1-e^{-\gamma x^c}\right)^{\rho}\right)}{(1-e^{-\gamma x^c})^{\rho}}\right)^{-(\alpha+1)}\sin\left\{\frac{\pi}{2}\left(1+\frac{\beta\left(1-\left(1-e^{-\gamma x^c}\right)^{\rho}\right)}{(1-e^{-\gamma x^c})^{\rho}}\right)^{-\alpha}\right\} \quad (59)$$

And the hazard function for CILEW is:

$$h(x) = \frac{\left(1+\frac{\beta\left(1-\left(1-e^{-\gamma x^c}\right)^{\rho}\right)}{(1-e^{-\gamma x^c})^{\rho}}\right)^{-(\alpha+1)}\sin\left\{\frac{\pi}{2}\left(1+\frac{\beta\left(1-\left(1-e^{-\gamma x^c}\right)^{\rho}\right)}{(1-e^{-\gamma x^c})^{\rho}}\right)^{-\alpha}\right\}}{\cos\left\{\frac{\pi}{2}\left(1+\frac{\beta(1-(1-e^{-\gamma x^c})^{\rho})}{(1-e^{-\gamma x^c})^{\rho}}\right)^{-\alpha}\right\}} \quad (60)$$

where $x, \alpha, \beta, \rho, c, \gamma > 0$

The PDF and hazard function plots of the CILEW distribution are presented in Figures 1a and 1b. From the PDF plot, it can be seen that the distribution is right-skewed, and from the hazard function plot, it is evident that the model exhibits increasing, and upside-down failure rate patterns.

V. SELECTED MODELS FOR EVALUATION

This section presents three special models of the CIL-G family, which generalize several well-known distributions. These models are derived using the Exponentiated Weibull (EW), Weibull (W), and Exponential (E) distributions as baseline distributions.

A. *The Cosine Inverse Lomax Exponentiated Weibull (CILEW) Distribution*

Consider the exponentiated Weibull distribution with a CDF of $G(x) = \left(1-e^{-\gamma x^c}\right)^{\rho}$ and PDF of $g(x) = \rho c\gamma x^{c-1}e^{-\gamma x^c}\left(1-e^{-\gamma x^c}\right)^{\rho-1}$ where $\gamma > 0$ is the scale parameter and $c, \rho > 0$ are the shape respectively, then the CDF of CILEW distribution is:

$$F(x) = 1 - \cos\left\{\frac{\pi}{2}\left(1+\frac{\beta\left(1-\left(1-e^{-\gamma x^c}\right)^{\rho}\right)}{\left(1-e^{-\gamma x^c}\right)^{\rho}}\right)^{-\alpha}\right\} \quad (58)$$

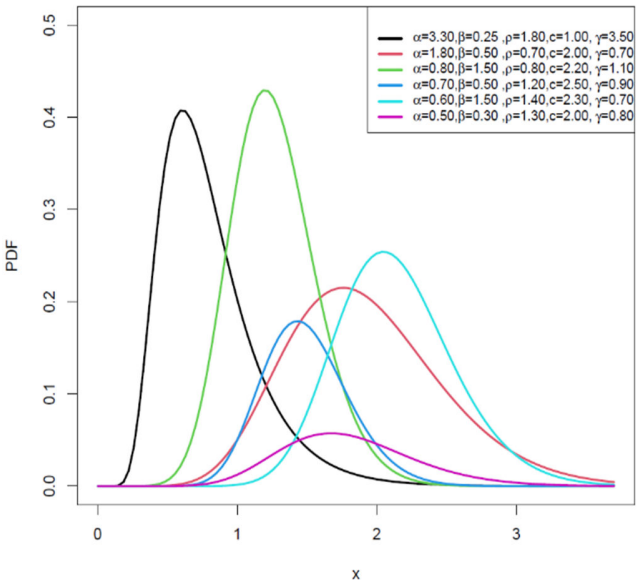

Figure 1a PDF plot of the CILEW distribution.

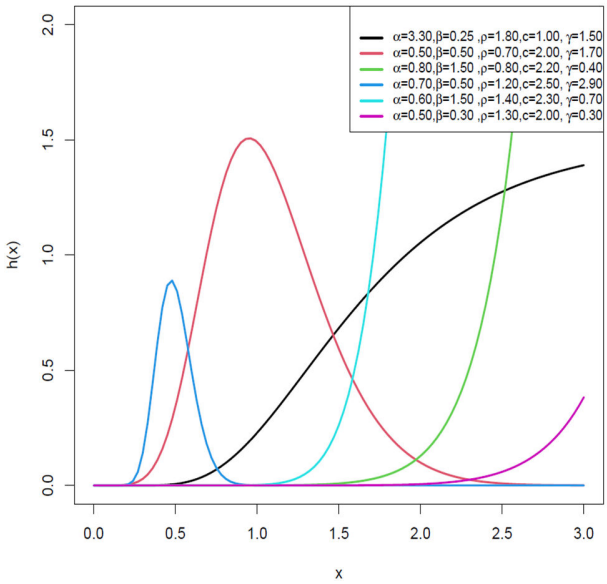

Figure 1b Hazard function plot of the CILEW distribution.

B. *The Cosine Inverse Lomax Weibull (CILW) Distribution*

The Weibull (W) distribution with parameter $d, a > 0$ has CDF and PDF given respectively, by

$$G(x) = 1 - e^{-\left(\frac{x}{a}\right)^d},\ g(x) = \left(\frac{d}{a}\right)\left(\frac{x}{a}\right)^{d-1} e^{-\left(\frac{x}{a}\right)^d}$$

Then the CDF and PDF of the CILW distribution is:

$$F(x) = 1 - \cos\left\{\frac{\pi}{2}\left(1 + \frac{\beta e^{-\left(\frac{x}{a}\right)^d}}{\left(1-e^{-\left(\frac{x}{a}\right)^d}\right)}\right)^{-\alpha}\right\} \tag{61}$$

$$f(x) = \frac{\pi}{2}\frac{\alpha\beta\left(\frac{d}{a}\right)\left(\frac{x}{a}\right)^{d-1} e^{-\left(\frac{x}{a}\right)^d}}{\left(1-e^{-\left(\frac{x}{a}\right)^d}\right)^2}\left(1 + \frac{\beta e^{-\left(\frac{x}{a}\right)^d}}{\left(1-e^{-\left(\frac{x}{a}\right)^d}\right)}\right)^{-(\alpha+1)} \sin\left\{\frac{\pi}{2}\left(1 + \frac{\beta e^{-\left(\frac{x}{a}\right)^d}}{\left(1-e^{-\left(\frac{x}{a}\right)^d}\right)}\right)^{-\alpha}\right\} \tag{62}$$

The hazard function for CILW is given below in Equation (64) as

$$h(x) = \frac{\frac{\pi}{2}\frac{\alpha\beta\left(\frac{d}{a}\right)\left(\frac{x}{a}\right)^{d-1} e^{-\left(\frac{x}{a}\right)^d}}{\left(1-e^{-\left(\frac{x}{a}\right)^d}\right)^2}\left(1 + \frac{\beta e^{-\left(\frac{x}{a}\right)^d}}{\left(1-e^{-\left(\frac{x}{a}\right)^d}\right)}\right)^{-(\alpha+1)} \sin\left\{\frac{\pi}{2}\left(1 + \frac{\beta e^{-\left(\frac{x}{a}\right)^d}}{\left(1-e^{-\left(\frac{x}{a}\right)^d}\right)}\right)^{-\alpha}\right\}}{\cos\left\{\frac{\pi}{2}\left(1 + \frac{\beta e^{-\left(\frac{x}{a}\right)^d}}{\left(1-e^{-\left(\frac{x}{a}\right)^d}\right)}\right)^{-\alpha}\right\}} \tag{63}$$

where $x, \alpha, \beta, d, a > 0$

The PDF and hazard function plots of the CILW distribution are presented in Figures 2a and 2b. The PDF plot shows that the CILW distribution is right-skewed, while the hazard function plot exhibits an increasing failure rate pattern.

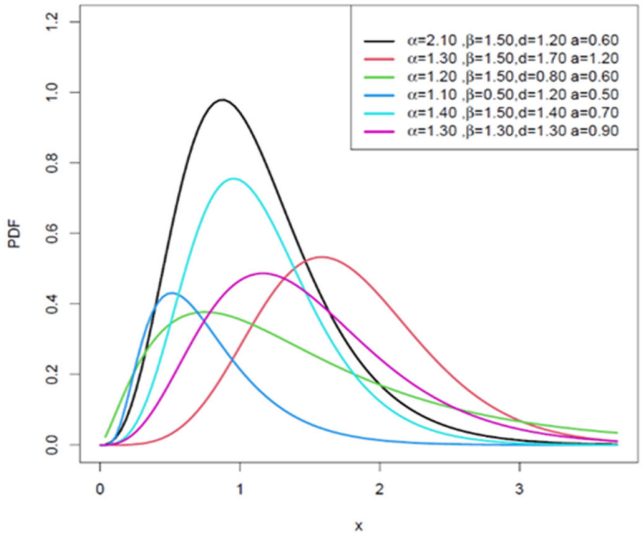

Figure 2a PDF plot of the CILW distribution.

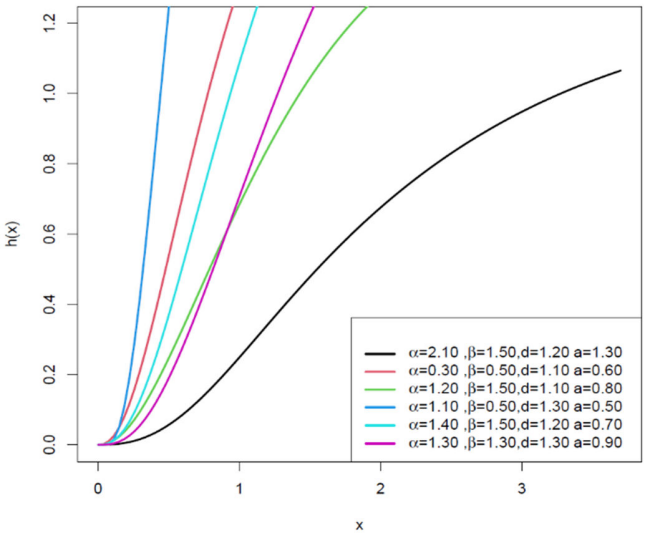

Figure 2b Hazard function plot of the CILW distribution.

C. *The Cosine Inverse Lomax Exponential (CILE) Distribution*

The Exponential (E) distribution with parameter $w > 0$ has CDF and PDF given respectively, by

$$G(x) = 1 - e^{-wx} \ , \ g(x) = we^{-wx} \qquad ; x > 0$$

Then the CDF and PDF of the CILE distribution are:

$$F(x) = 1 - \cos\left\{\frac{\pi}{2}\left(1 + \frac{\beta e^{-wx}}{1-e^{-wx}}\right)^{-\alpha}\right\} \tag{64}$$

$$f(x) = \frac{\pi}{2}\frac{\alpha\,\beta\,we^{-wx}}{(1-e^{-wx})^2}\left(1 + \frac{\beta e^{-wx}}{1-e^{-wx}}\right)^{-(\alpha+1)} \sin\left\{\frac{\pi}{2}\left(1 + \frac{\beta e^{-wx}}{1-e^{-wx}}\right)^{-\alpha}\right\}, x, \alpha, \beta, w > 0 \tag{65}$$

The hazard function for CILE is

$$h(x) = \frac{\frac{\pi}{2}\frac{\alpha\,\beta\,we^{-wx}}{(1-e^{-wx})^2}\left(1 + \frac{\beta e^{-wx}}{1-e^{-wx}}\right)^{-(\alpha+1)} \sin\left\{\frac{\pi}{2}\left(1 + \frac{\beta e^{-wx}}{1-e^{-wx}}\right)^{-\alpha}\right\}}{\cos\left\{\frac{\pi}{2}\left(1 + \frac{\beta e^{-wx}}{1-e^{-wx}}\right)^{-\alpha}\right\}} \tag{66}$$

where $x, \alpha, \beta, d, a > 0$

The PDF and hazard function plots of the CILE distribution are presented in Figures 3a and 3b. The PDF plot shows that the CILE distribution is right-skewed, while the hazard function plot exhibits an increasing failure rate pattern.

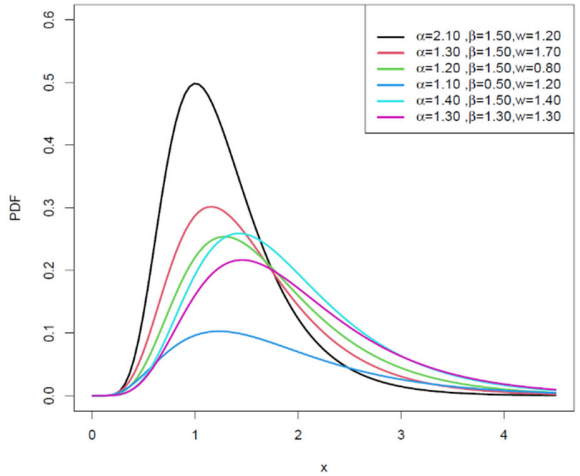

Figure 3a PDF plot of the CILE distribution.

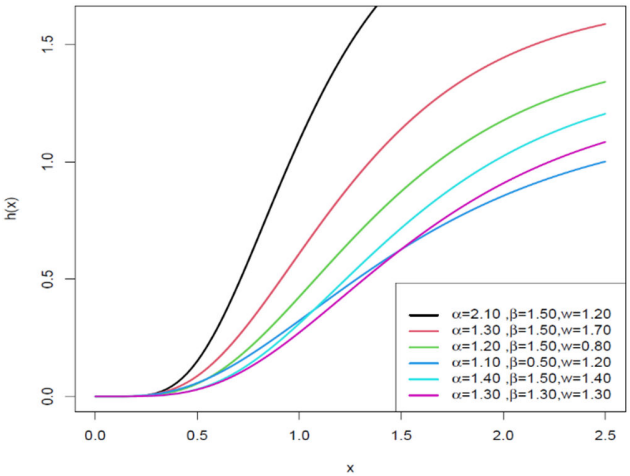

Figure 3b Hazard function plot of the CILE distribution.

VI. SIMULATION

This section presents and discusses the findings from the CILEW distribution simulation study. The study explores three different parameter combinations: (α=2, β=2.5, ρ=1.2, c=0.5, γ=0.01), (α=2.1, β=2.6, ρ=1.4, c=0.5, γ=0.002), and (α=2.3, β=2.7, ρ=1.1, c=0.5, γ=0.002). For each parameter set, one thousand random samples were generated using the inverse transform method. Specifically, uniform random variables U(0,1) were drawn and transformed using the quantile function (inverse CDF) of the CILEW distribution. This process was implemented in R software version 4.4.2. The simulations were conducted for sample sizes n=100, 200, 300, and 400. The calculations for average bias and root mean square error (RMSE) are based on these generated samples.

As the sample size n increases, the RMSE and bias for each estimator decrease as shown in Tables 1, 2, and 3, demonstrating the consistency of the estimators.

Table 1. Monte Carlo simulation results for the CILEW distribution with parameters α=2, β=2.5, ρ=1.2, c=0.5, γ=0.01.

n		Est. Par.	MLE	LSE	WLSE
100	RMSE	α	2.85513	2.96494	2.88305
		β	5.71271	2.91948	3.86237
		ρ	2.60628	1.35488	1.73383
		c	0.18500	0.05721	0.05006
		γ	0.02439	0.01313	0.01084
	Bias	α	1.54013	0.79061	0.60678
		β	2.44152	0.72441	0.83325
		ρ	0.28951	0.50198	0.65385
		c	0.00741	0.00524	0.00613
		γ	0.00605	0.00408	0.00340
200	RMSE	α	1.99095	1.81149	2.34260
		β	5.41493	2.06202	2.06707
		ρ	2.17979	1.15362	1.05194
		c	0.16407	0.04007	0.03447
		γ	0.09974	0.00802	0.00689
	Bias	α	1.20625	0.37300	0.39107
		β	1.74871	0.31907	0.41716
		ρ	0.11480	0.39545	0.38677
		c	0.00710	0.00456	0.00244
		γ	0.00359	0.00192	0.00125
300	RMSE	α	0.11936	1.50785	1.50785
		β	4.31629	2.00855	2.01855
		ρ	2.07030	1.05689	1.05089
		c	0.11316	0.03553	0.03253
		γ	0.01424	0.00642	0.00642
	Bias	α	1.21678	0.37093	0.37893
		β	1.18685	0.24162	0.44162
		ρ	0.11236	0.26488	0.26488
		c	0.01039	0.00095	0.00095
		γ	0.00801	0.00136	0.00136
400	RMSE	α	0.02516	1.11091	1.12078
		β	4.13630	1.63687	1.52234
		ρ	1.33295	0.75035	0.64708
		c	0.10265	0.02776	0.02356
		γ	0.01122	0.00412	0.00358
	Bias	α	1.05527	0.19854	0.21101
		β	1.07443	0.14992	0.25918
		ρ	0.10061	0.22225	0.19817
		c	0.00758	0.00044	0.00042
		γ	0.00604	0.00061	0.00055

Table 2. Monte Carlo simulation results for the CILEW distribution with parameters α=2.1, β=2.6, ρ=1.4, c=0.5, γ=0.002.

n		Est. Par.	MLE	LSE	WLSE
100	RMSE	α	4.02445	2.71106	1.83603
		β	3.09569	2.79068	2.83856
		ρ	1.88171	1.50699	1.87498
		c	0.13520	0.04339	0.04165
		γ	0.56154	0.00188	0.00836
	Bias	α	1.29970	0.45530	0.34705
		β	0.10499	0.61004	0.71926
		ρ	0.12836	0.48277	0.67978
		c	0.08612	0.00323	0.00374
		γ	0.04573	0.00039	0.00031
200	RMSE	α	2.16810	1.65544	1.65993
		β	0.69944	2.02337	2.06901
		ρ	1.10470	1.18257	1.09715
		c	0.12966	0.03487	0.03538
		γ	0.00198	0.00142	0.00138
	Bias	α	1.08935	0.36155	0.34551
		β	0.02162	0.50072	0.62689
		ρ	0.0638	0.40387	0.41529
		c	0.07780	0.00147	0.00350
		γ	0.00198	0.00029	0.00022
300	RMSE	α	2.12156	1.45628	1.38123
		β	0.69042	2.01859	1.75122
		ρ	0.83559	0.97401	0.87194
		c	0.12803	0.02900	0.02663
		γ	0.00196	0.00116	0.00127
	Bias	α	1.02283	0.28865	0.28880
		β	0.18672	0.48901	0.38490
		ρ	0.05114	0.32201	0.25115
		c	0.07284	0.00127	0.00217
		γ	0.00195	0.00028	0.00012
400	RMSE	α	2.11597	1.23867	1.19106
		β	0.64088	1.15375	1.15221
		ρ	0.81286	0.70829	0.71755
		c	0.12557	0.02442	0.02518
		γ	0.00194	0.00087	0.00109
	Bias	α	1.01008	0.28382	0.23781
		β	0.17466	0.42827	0.37893
		ρ	0.03824	0.13449	0.17303
		c	0.03179	0.00113	0.00118
		γ	0.00191	0.00011	0.00011

Table 3. Monte Carlo simulation results for the CILEW distribution with parameters α=2.3, β=2.7, ρ=1.1, c=0.5, γ=0.002.

n		Est. Par.	MLE	LSE	WLSE
		α	5.78822	2.96836	2.59912
	RMSE	β	2.53657	2.73960	2.66450
		ρ	1.35775	1.14676	1.35761
		c	0.13121	0.04551	0.04437
100		γ	0.07778	0.00197	0.00199
		α	1.46942	1.36393	0.63373
		β	0.34908	0.63164	0.63071
	Bias	ρ	0.12898	0.47404	0.52711
		c	0.08700	0.00347	0.00168
		γ	0.00606	0.00042	0.00051
		α	2.68696	2.11944	2.09858
		β	0.73057	2.55087	2.44404
	RMSE	ρ	1.12796	0.88507	0.93503
		c	0.13074	0.03750	0.03400
200		γ	0.00199	0.00164	0.00142
		α	1.32299	0.51372	0.45788
		β	0.06282	0.51962	0.55745
		ρ	0.16727	0.33333	0.29035
	Bias	c	0.09237	0.00210	0.00149
		γ	0.00198	0.00041	0.00033
		α	1.86942	1.50240	1.83132
		β	0.69137	1.98484	1.62133
		ρ	0.99011	0.60268	0.74405
300		c	0.12216	0.02877	0.02878
	RMSE	γ	0.00197	0.00112	0.00124
		α	1.06427	0.25408	0.35410
		β	0.21445	0.42890	0.31455
	Bias	ρ	0.05141	0.20742	0.24057
		c	0.08687	0.00190	0.00109
		γ	0.00196	0.00028	0.00028
		α	1.80169	1.42755	1.31825
		β	0.66794	1.64724	1.44998
		ρ	0.48231	0.56852	0.62473
400	RMSE	c	0.12042	0.02758	0.02686
		γ	0.00190	0.00105	0.00100
		α	1.03969	0.19581	0.32046
		β	0.03898	0.30353	0.26288
		ρ	0.02886	0.13755	0.15491
	Bias	c	0.08170	0.00033	0.00028
		γ	0.00193	0.00019	0.00018

VII. APPLICATION

To evaluate the effectiveness of the CILEW distribution, we conduct an empirical analysis using three real-world datasets from engineering and medical fields. The CILEW distribution is fitted to these datasets and compared against several competing models, including the truncated exponentiated exponential exponentiated Weibull (TEEEW) distribution, the beta exponentiated Weibull (BeEW) distribution (Cordeiro et al., 2013), the Kumaraswamy exponentiated Weibull (KuEW) distribution, the exponential generalized exponentiated Weibull (EGEW) distribution, the Weibull exponentiated Weibull (WeEW) distribution, and the exponentiated Weibull (EW) distribution (Hassan et al., 2017). The cumulative distribution functions (CDFs) of these models are given in Table 4.

Table 4. CDFs of the Competing Models

Competing Models	CDF
TEEEW	$\frac{\left(1-exp\left(\left(-\beta\left(1-exp(-(\gamma x)^c)\right)^\rho\right)\right)\right)^\alpha}{\left(1-exp(-\alpha)\right)^\rho}$
BeEW	$\rho\beta\left(\left(1-exp(-(\gamma x)^c)\right)^\rho,\beta,\alpha\right)$
KuEW	$1-\left(1-\left(1-exp(-(\gamma x)^c)\right)^\rho\right)^{\beta\alpha}$
EGEW	$\left(1-\left(1-\left(1-exp(-(\gamma x)^c)\right)^\rho\right)^\beta\right)^\alpha$
WeEW	$1-exp\left(-(\alpha)^{-\beta}\left(-log\left(1-\left(1-exp(-(\gamma x)^c)\right)^\rho\right)\right)^\alpha\right)$
EW	$\left(1-exp(-(\gamma x)^c)\right)^\rho$

A) Data Collection

The datasets used in this study are secondary data obtained from existing literature and publicly available sources. They were selected to demonstrate the applicability of the CILEW distribution in modelling engineering and medical data. Below is a description of each dataset and its source.

1. **Data A**: This dataset represents the time to failure of 40 turbocharger units in diesel engines. The data was obtained from Alobaidi *et al.* (2021). The dataset includes 40 observations. The observations are as follows:

1.6, 3.5,4.8,5.4,6.0, 6.5, 7.0, 7.3, 7.7,8.0, 8.4, 2.0, 3.9, 5.0 ,5.6 ,6.1 ,6.5 ,7.1 ,7.3, 7.8,8.1, 8.4, 2.6, 4.5, 5.1, 5.8, 6.3, 6.7 ,7.3,7.7, 7.9, 8.3, 8.5, 3.0, 4.6, 5.3, 6.0, 8.7 ,8.8, 9.0

2. **Data B**: This dataset provides information on the duration of pain relief, measured in minutes, for 20 individuals who took analgesics. The data was sourced from Hassan et al. (2020). The dataset includes 20 observations.

The recorded durations are as follows:

1.1, 1.4, 1.3, 1.7, 1.9, 1.8, 1.6, 2.2, 1.7, 2.7, 4.1, 1.8, 1.5, 1.2, 1.4, 3.0, 1.7, 2.3, 1.6 2.0.

3. **Data C**: This dataset estimates the time from growth hormone treatment to target age in children. The data was obtained from Oluyede *et al.* (2020). The dataset includes 35 observations.

2.15, 2.20, 2.55, 2.56, 2.63, 2.74, 2.81, 2.90, 3.05, 3.41, 3.43, 3.43, 3.84, 4.16, 4.18, 4.36, 4.42, 4.51,4.60, 4.61, 4.75, 5.03, 5.10, 5.44, 5.90, 5.96, 6.77, 7.82, 8.00, 8.16, 8.21, 8.72, 10.40, 13.20, 13.70.

B) Data Analysis

The analysis of the datasets was carried out using the CILEW distribution and several other competitive models, including TEEEW, BeEW, KuEW, EGEW, WeEW, and EW. The goal of the analysis is to evaluate the goodness-of-fit of the CILEW distribution compared to these models. The analysis was conducted using R programming software version 4.4.2. The descriptive statistics of datasets A, B, and C are presented in Tables 4, 6, and 8, respectively. The visual representations of the datasets are provided in Figures 4a, 7b, and 10c. Each dataset was fitted with the CILEW distribution and the competing models. The maximum likelihood estimation (MLE) method was used to estimate the parameters of each model. The MLEs for each model are provided in Tables 5, 7, and 9 for datasets A, B, and C, respectively. To compare the performance of the models, several goodness-of-fit metrics were calculated, including the AIC, CAIC, BIC, HQIC, and the maximized log-likelihood (-2L). Additionally, the Cramer-von Mises (W), Anderson-Darling (A), KS, and P-value statistics were considered. Lower values for AIC, CAIC, BIC, HQIC, W, A, and KS, along with higher P-values, indicate a better model fit.

The fitted models were visually compared using histograms, empirical cumulative distribution functions (ECDF), Kaplan-Meier survival (Kaplan-MS) plots, and probability-probability (PP) plots. These visualizations help in assessing how well the models fit the data. The results of the goodness-of-fit metrics are presented in Tables 5, 7, and 9 for datasets A, B, and C, respectively. The visual comparisons are presented in Figures 5a, 5b, 8a, 8b, 11a, and 11b for the three datasets.

1) Analysis results for the first dataset

The descriptive statistics of dataset A in Table 5 indicate that the data is moderately negatively skewed. This observation is further supported by the plots in Figure 4a.

Table 5. Descriptive Statistics of Dataset A

n	Mean	Median	Mode	Skewness	Kurtosis
40	6.25	6.5	2.08	-0.64	-0.49

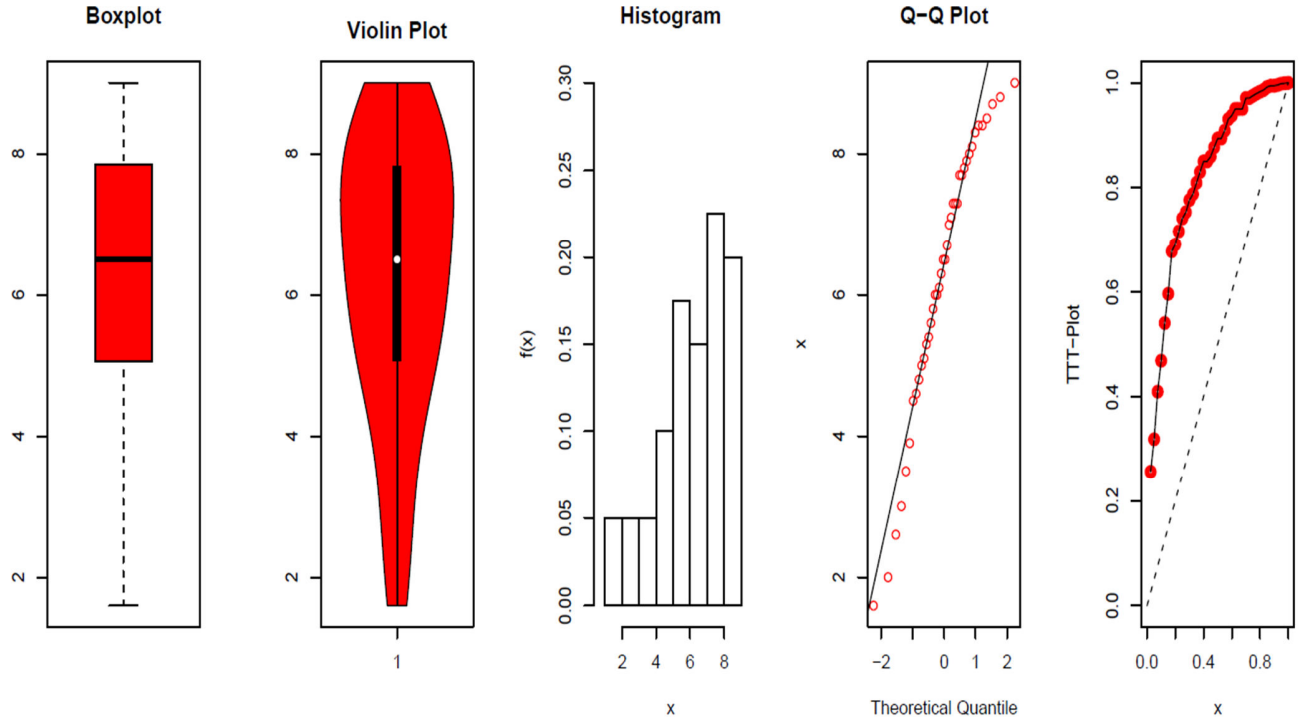

Figure 4a. Box plot, violin plot, histogram, Q-Q plot, and TTT plot of dataset A

The goodness-of-fit test results in Table 6 indicate that the CILEW distribution outperforms the competing models in fitting the first dataset. This is evidenced by its lowest AIC, CAIC, BIC, HQIC, W, A, and KS values, along with the highest associated KS p-value. Collectively, these metrics confirm that the CILEW distribution provides the best fit for the data. Further evidence of this is provided by the PDF and ECDF plots in Figure 5, which show that the CILEW model aligns more closely with the empirical data than the competing models. Additionally, the survival function and probability-probability (P-P) plots in Figure 6 reinforce this finding, demonstrating that the proposed CILEW model closely fits the data.

Table 6. The goodness-of-fit results for the data A

Model	MLEs	-2L	AIC	CAIC	BIC	HQIC	W	A	KS (p-value)
CILEW	$\hat{\alpha}$: 5.4305 $\hat{\beta}$: 2.2027 $\hat{\rho}$:0.0026 $\hat{c}$:9.3787 $\hat{\gamma}$:0.1205	80.81	171.62	173.39	180.07	174.68	0.0246	0.1941	0.0931 (0.8786)
TEEEW	$\hat{\alpha}$:0.6426 $\hat{\beta}$:1.3606 $\hat{\rho}$:1.5128 $\hat{c}$2.5314 $\hat{\gamma}$:0.1684	85.75	181.53	183.30	189.98	184.58	0.1604	1.0963	0.1158 (0.6558)
BeEW	$\hat{\alpha}$:1.4409 $\hat{\beta}$:0.9453 $\hat{\rho}$1.3898 $\hat{c}$:2.3222 $\hat{\gamma}$:0.18365	84.99	180.05	181.81	188.49	183.10	0.1403	0.9753	0.1222 (0.5886)
KuEW	$\hat{\alpha}$:1.1670 $\hat{\beta}$:1.1507 $\hat{\rho}$:1.1670 $\hat{c}$:2.8805 $\hat{\gamma}$:0.1515	83.65	177.33	179.10	185.78	180.38	0.1075	0.7713	0.1112 (0.7048)
EGEW	$\hat{\alpha}$:0.5471 $\hat{\beta}$:1.5124 $\hat{\rho}$:0.7848 $\hat{c}$3.1755 $\hat{\gamma}$:0.1875	83.00	176.12	177.88	184.56	179.17	0.0924	0.6743	0.1142 (0.6730)
WeEW	$\hat{\alpha}$:1.8011 $\hat{\beta}$:0.9570 $\hat{\rho}$:1.3283 $\hat{c}$:1.7740 $\hat{\gamma}$:0.1597	83.05	176.11	177.88	184.56	179.17	0.0912	0.6672	0.1104 (0.7134)
EW	$\hat{\rho}$:1.9070 $\hat{c}$:2.1063 $\hat{\gamma}$:0.1819	85.66	177.33	178.00	182.40	179.16	0.1480	1.0225	0.1313 (0.4950)

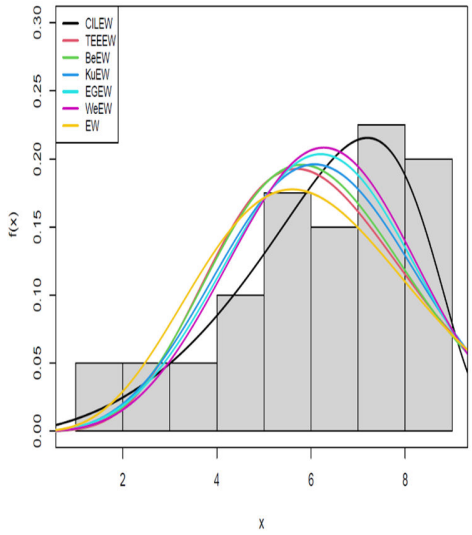

Figure 5a Estimated PDFs for data A

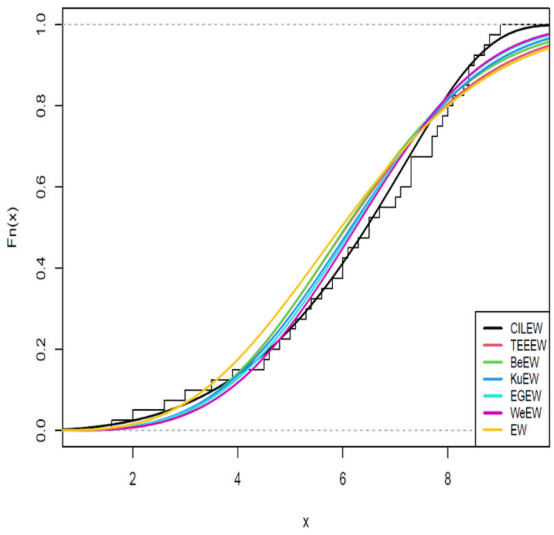

Figure 5b Estimated CDFs for data A

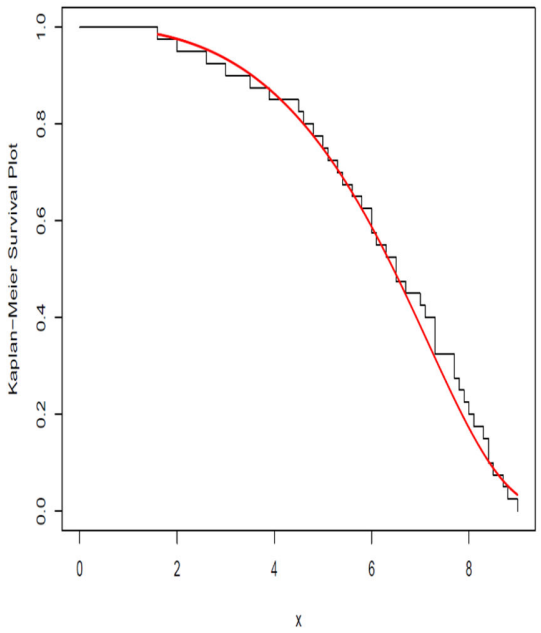

Figure 6a Kaplan-MS plot for data A

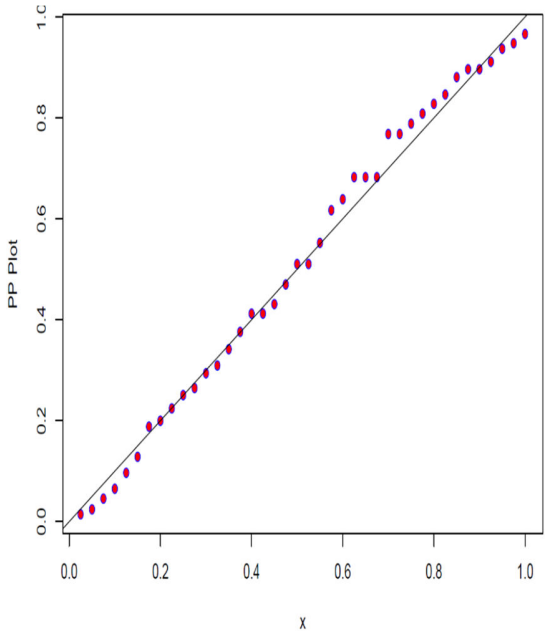

Figure 6b PP plot for data A.

2) Analysis results for the second dataset

The descriptive statistics of Dataset B in Table 7 indicate that the data is highly positively skewed. This observation is further supported by the plots in Figure 7b.

Table 7: Descriptive Statistics of Dataset B

n	Mean	Median	Mode	Skewness	Kurtosis
20	1.90	1.70	1.70	1.86	4.19

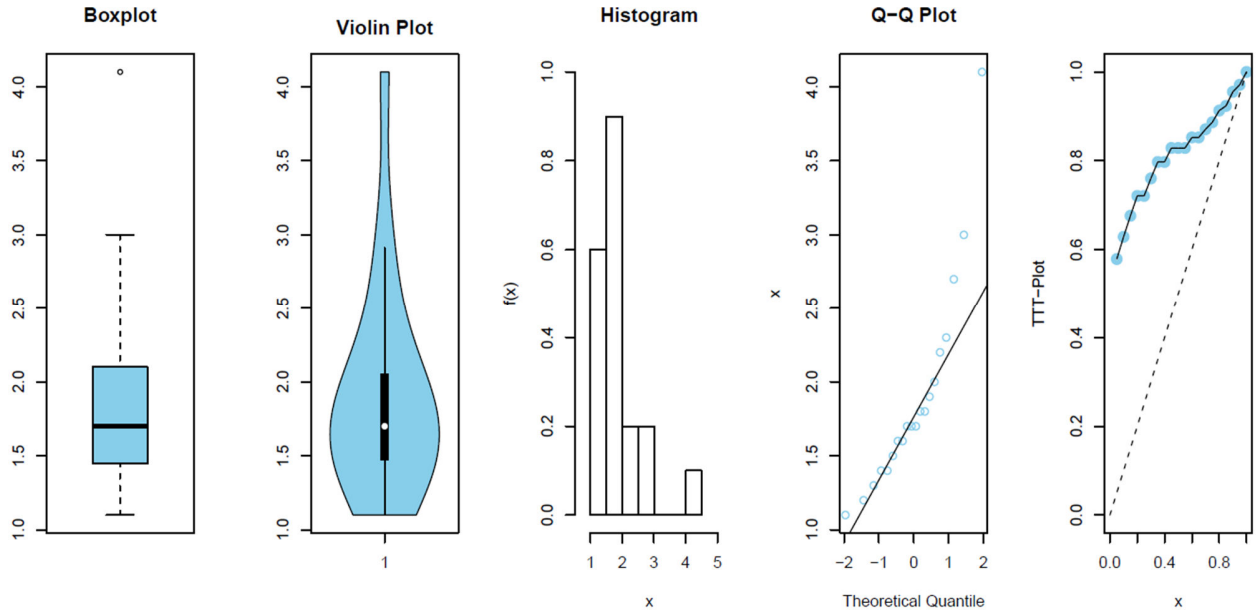

Figure 7b. Box plot, violin plot, histogram, Q-Q plot, and TTT plot of dataset B

The goodness-of-fit test results in Table 8 indicate that the CILEW distribution outperforms the competing models in fitting the second dataset. This is evidenced by its lowest AIC, CAIC, BIC, HQIC, W, A, and KS values, along with the highest associated KS p-value. Collectively, these

metrics confirm that the CILEW distribution provides the best fit to the data. Additional support for this is provided by the PDF and ECDF plots in Figure 8, which show that the CILEW model aligns more closely with the empirical data than the competing models. The survival function and P-P plots in Figure 9 closely follow the empirical data, further demonstrating the model's strong fit.

Table 8. The goodness-of-fit results for the Data B

Model	MLEs	-2L	AIC	CAIC	BIC	HQIC	W	A	K-S (p-value)
CILEW	$\hat{\alpha}$:1.8902 $\hat{\beta}$:3.3037 $\hat{\rho}$:0.6908 $\hat{c}$:.4898 $\hat{\gamma}$:3.1302	15.54	41.096	45.381	46.074	42.068	0.0315	0.1807	0.1103 (0.9680)
TEEEW	$\hat{\alpha}$:2.3334 $\hat{\beta}$: 2.6174 $\hat{\rho}$:2.9645 $\hat{c}$:1.5962 $\hat{\gamma}$:0.7457	16.27	42.559	46.845	47.538	43.531	0.0562	0.3342	0.1412 (0.8198)
BeEW	$\hat{\alpha}$:5.0058 $\hat{\beta}$: 0.5167 $\hat{\rho}$:4.8485 $\hat{c}$:1.2806 $\hat{\gamma}$:1.8181	16.09	42.283	46.569	47.262	43.255	0.0526	0.3094	0.1502 (0.7570)
KuEW	$\hat{\alpha}$:4.1756 $\hat{\beta}$: 0.3881 $\hat{\rho}$:4.1756 $\hat{c}$:1.5672 $\hat{\gamma}$:1.4613	16.27	42.562	46.848	47.541	43.534	0.0584	0.3447	0.1511 (0.7510)
EGEW	$\hat{\alpha}$:1.0286 $\hat{\beta}$:4.4054 $\hat{\rho}$:4.3191 $\hat{c}$:1.1131 $\hat{\gamma}$:1.6168	16.52	43.052	47.338	48.030	44.0242	0.0642	0.3790	0.1461 (0.7867)
WeEW	$\hat{\alpha}$:0.4297 $\hat{\beta}$:1.1434 $\hat{\rho}$:4.4153 $\hat{c}$:3.6483 $\hat{\gamma}$:0.6465	16.17	42.340	46.626	47.319	43.312	0.0445	0.2672	0.1304 (0.8853)
EW	$\hat{\rho}$:2.4085 $\hat{c}$:2.0263 $\hat{\gamma}$:0.6332	18.671	43.347	44.847	46.334	43.930	0.1313	0.7778	0.1837 (0.5089)

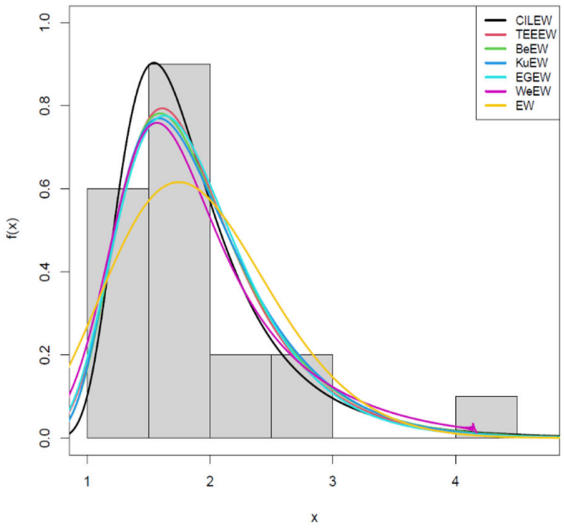

Figure 8a Estimated PDFs for data B

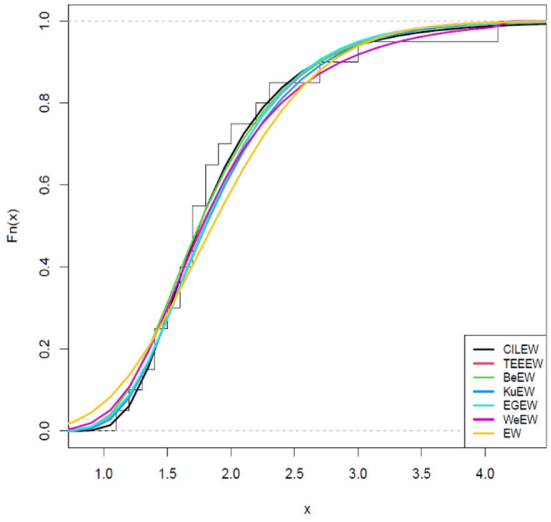

Figure 8b Estimated CDFs for data B

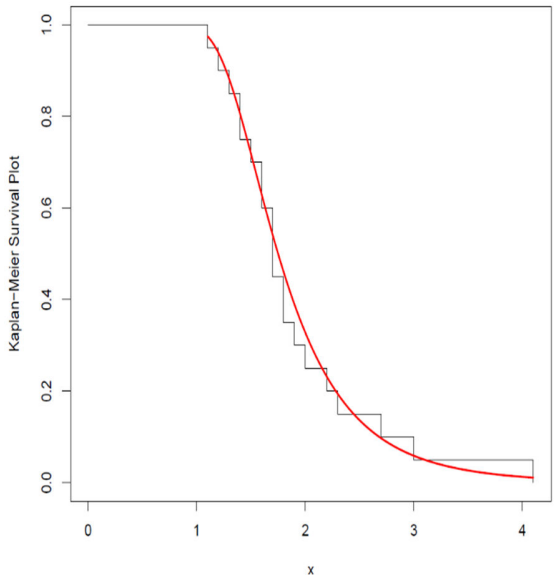

Figure 9a Kaplan-MS plot for data B

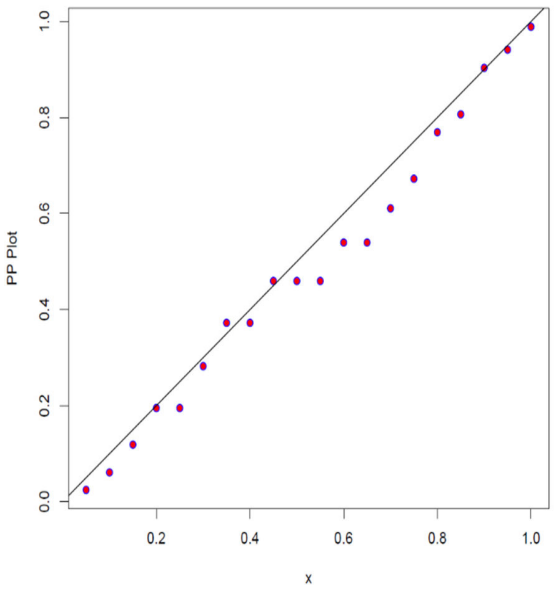

Figure 9b PP plot for data B.

3) Analysis Results for the third Dataset

The descriptive statistics of dataset C in Table 9 indicate that the data is highly positively skewed. This observation is further supported by the plots in Figure 10c.

Table 9: Descriptive Statistics of Dataset C

n	Mean	Median	Mode	Skewness	Kurtosis
35	5.31	4.51	3.43	1.43	1.82

The goodness-of-fit test results in Table 10 indicate that the CILEW distribution outperforms the competing models in fitting the third dataset. This is evidenced by its lowest AIC, CAIC, BIC, HQIC, W, A, and KS values, along with the highest associated KS p-value. Collectively, these metrics confirm that the CILEW distribution provides the best fit to the data. Additional support for this is provided by the histogram and ECDF plots in Figure 11, which show that the CILEW model aligns more closely with the empirical data than the competing models. The survival function and P-P plots in Figure 12 further validate this result, demonstrating that the proposed CILEW model closely fits the data.

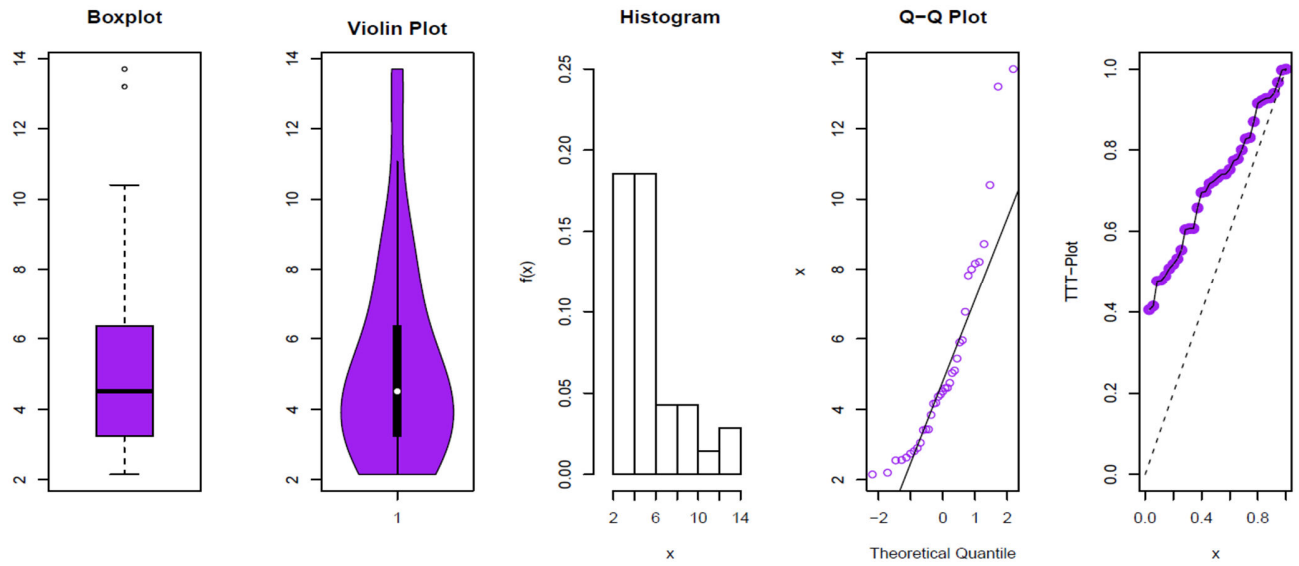

Figure 10c. Box plot, violin plot, histogram, Q-Q plot, and TTT plot of dataset C

Table 10. The goodness-of-fit results for the data C

Model	MLEs	-2L	AIC	CAIC	BIC	HQIC	W	A	K-S (p-value)
CILEW	$\hat{\alpha}$:4.4339 $\hat{\beta}$:4.3307 $\hat{\rho}$:0.1100 $\hat{c}$:0.3712 $\hat{\gamma}$:3.2972	77.72	165.44	167.51	173.22	168.13	0.0349	0.2539	0.0844 (0.9640)
TEEEW	$\hat{\alpha}$:1.2822 $\hat{\beta}$:1.7779 $\hat{\rho}$:1.8858 $\hat{c}$:1.3411 $\hat{\gamma}$:0.2468	79.16	168.34	170.40	176.11	171.02	0.0734	0.4954	0.1001 (0.8743)
BeEW	$\hat{\alpha}$:2.2484 $\hat{\beta}$:0.2353 $\hat{\rho}$:2.2057 $\hat{c}$:1.4437 $\hat{\gamma}$:0.6194	78.70	167.42	169.49	175.20	170.10	0.0656	0.4468	0.1011 (0.8664)
KuEW	$\hat{\alpha}$:2.4637 $\hat{\beta}$:0.2491 $\hat{\rho}$:2.4637 $\hat{c}$:1.3950 $\hat{\gamma}$:0.6269	78.51	167.07	169.14	174.85	169.75	0.0622	0.4247	0.0995 (0.8784)
EGEW	$\hat{\alpha}$:0.5620 $\hat{\beta}$:2.4682 $\hat{\rho}$:2.6128 $\hat{c}$:1.0577 $\hat{\gamma}$:0.6773	78.97	167.97	170.04	175.74	170.65	0.0693	0.4682	0.0999 (0.8774)
WeEW	$\hat{\alpha}$:1.0756 $\hat{\beta}$:1.0866 $\hat{\rho}$:1.8870 $\hat{c}$:1.4001 $\hat{\gamma}$:0.2416	80.91	171.84	173.91	179.62	174.53	0.1215	0.7762	0.1303 (0.5912)
EW	$\hat{\rho}$:1.8322 $\hat{c}$:1.5328 $\hat{\gamma}$:0.2227	80.92	167.85	168.62	172.51	169.46	0.1225	0.7821	0.1321 (0.5740)

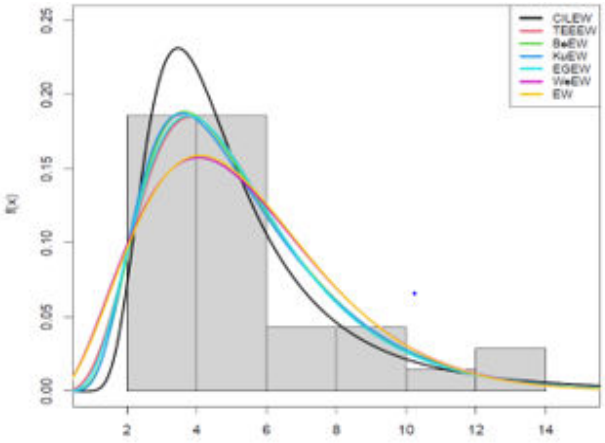

Figure 11a Estimated PDFs for data C

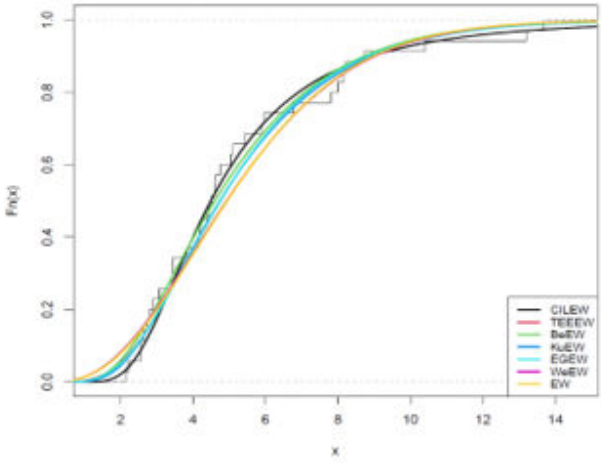

Figure 11b Estimated CDFs for data C

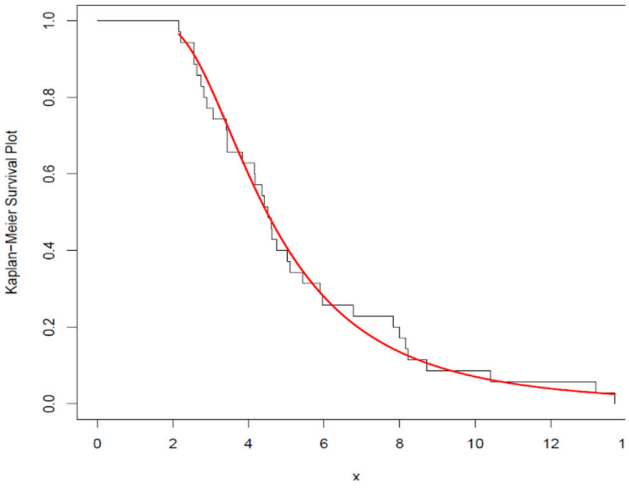

Figure 12a Kaplan-MS plot for data C

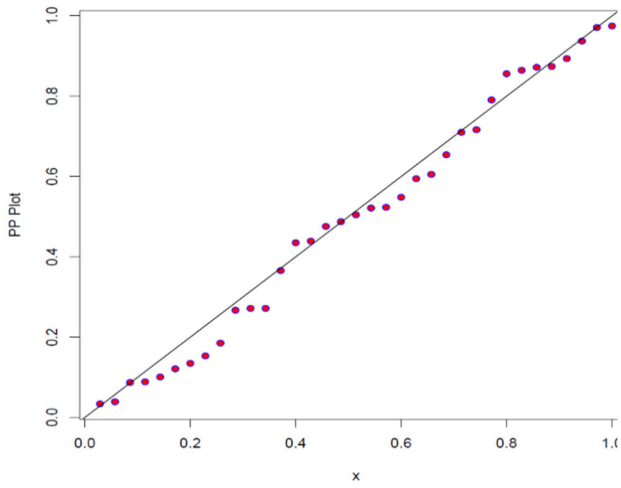

Figure 12b PP plot for data C.

VIII. RESULTS AND DISCUSSION

In this study, the CIL family of distributions is introduced, and its cumulative distribution function (CDF) and probability density function (PDF) are derived, and presented in Equations 5 and 6 respectively. Several statistical properties of the CIL family are established; they include the survival function, hazard function, quantile function, moments, Rényi entropy, and linear representation. The parameters of the distribution family were estimated using three classical methods: maximum likelihood estimation, least squares estimation, and weighted least squares estimation. Furthermore, three sub-models of the proposed family were derived using the Exponentiated Weibull (EW), Weibull (W), and Exponential (E) distributions as baseline models. For the first sub-model, the CILEW distribution, the probability density function (PDF) and hazard function plots were presented in Figures 1a and 1b. The PDF plot indicates that the CILEW distribution exhibits right skewness. Additionally, the hazard function plots reveal both an upside-down bathtub shape and a monotonically increasing trend. These characteristics make the model particularly useful for analysing datasets with varying hazard rates. In engineering, a monotonically increasing hazard rate can model the failure times of aging infrastructure, where the risk of failure grows over time due to wear and tear. In medicine, the upside-down bathtub shape can represent the risk of disease recurrence, which peaks after treatment and then declines as the patient recovers.

In finance, the right-skewed PDF can model the time to loan default, where most defaults occur after a prolonged period of financial stress. For the second sub-model, the CILW distribution, the PDF and hazard function plots are shown in Figures 2a and 2b. The PDF plot confirms that the

model is positively skewed, while the hazard function plot demonstrates a monotonically increasing hazard rate. These characteristics make the model suitable for analysing datasets across various fields. For the third sub-model, the CILE distribution, the PDF and hazard function plots are presented in Figures 3a and 3b. The PDF plot shows that the model is right-skewed, while the hazard function plot reveals a monotonically increasing hazard rate. These properties further expand the applicability of the CIL family of distributions to a wide range of real-world scenarios. A simulation analysis is conducted to assess the performance of the CILEW distribution. The analysis involves simulating random variables with different parameter values and sample sizes (100, 200, 300, and 400.).

Tables 1 to 3 present the maximum likelihood estimates, least squares estimates, and weighted least squares estimates, along with their respective bias and root mean squared error (RMSE). Notably, the estimates obtained using the three techniques consistently exhibit decreasing bias and RMSE with increasing sample sizes. The decreasing bias and RMSE values with increasing sample sizes highlight the reliability and robustness of the estimation techniques for the CILEW distribution. To assess the practical utility of the CILEW model, it was applied to three real-life datasets from engineering and medical fields, and its performance was compared with six competing models. The first dataset, from engineering, represents the failure times of 40 turbocharger units in diesel engines. The second dataset, from the medical field, records the duration of pain relief for individuals who took analgesics. The third dataset estimates the time from growth hormone treatment initiation to the attainment of the target age in children. The descriptive statistics of the first dataset, presented in Table 5, indicate moderate negative skewness. Similarly, Table 7 shows that the second dataset is highly positively skewed, while Table 9 reveals that the third dataset also exhibits high positive skewness.

The box plot, violin plot, and histogram in Figure 4a confirm that the first dataset is moderately negatively skewed, while the TTT plot indicates a monotonically increasing hazard rate pattern, and the Q-Q plot shows that the data deviate from normality. Likewise, the box plot, violin plot, and histogram in Figure 7b demonstrate that the second dataset is highly positively skewed, the TTT plot confirms an increasing hazard rate pattern, and the Q-Q plot indicates that the data deviate from normality. Finally, Figure 10c shows that the third dataset is highly positively skewed, as evidenced by the box plot, violin plot, and histogram, while the TTT plot indicates an increasing hazard rate pattern, and the Q-Q plot confirms that the data deviate from normality. The goodness-of-fit results, is presented in Tables 6, 8, and 10, demonstrate that the proposed model outperforms the competing models across all three datasets. Specifically, the CILEW model achieves the lowest values for AIC, CAIC, BIC, HQIC, A, W and KS while attaining the highest P-values among all models.

The estimated probability density function (PDF) and cumulative distribution function (CDF) plots in Figures 5a, 5b, 8a, 8b, 11a, and 11b reinforce these findings, demonstrating that the proposed model aligns more closely with the empirical data than the competing models. Additionally, the estimated survival function and PP plots in Figures 6a, 6b, 9a, 9b, 12a, and 12b illustrate how well the proposed model fits the observed data. The superior performance of the CILEW model has important implications. First, its ability to accurately fit datasets with varying skewness patterns highlights its flexibility and robustness in modelling real-world phenomena. This makes it particularly valuable in reliability engineering, where precise failure-time predictions can enhance maintenance scheduling and risk assessment. In medical applications, the model's effectiveness in capturing pain relief duration and treatment response time suggests its potential utility in clinical decision-making and pharmaceutical research. By outperforming existing models, the CILEW model contributes to the development of more accurate predictive tools, ultimately improving decision-making in both engineering and healthcare domains.

IX. CONCLUSION

In this study, we introduced a novel hybrid family of distributions, the cosine inverse Lomax generated family, derived by combining the cosine and inverse Lomax distribution families. We examined various properties of this model, including the survival function, hazard function, moments, Rényi entropy, and order statistics. Additionally, we explored three special cases, using the exponentiated Weibull, Weibull, and exponential distributions as baseline models. The parameters of the new family were estimated using maximum likelihood, least squares, and weighted least squares methods. The application of one of the sub-models, the CIL-exponentiated Weibull, to engineering and medical datasets demonstrated its strong alignment with the dataset's characteristics. The model outperformed several competing models across multiple evaluation metrics, showcasing its effectiveness in modelling real-world data. By introducing this new family of distributions, our study enhances the flexibility of existing models, particularly through its ability to accommodate varying hazard function shapes. This flexibility makes the family suitable for a wide range of data types, from reliability engineering to healthcare analytics. For healthcare professionals and policymakers, the accuracy and adaptability of this model can support more effective decision-making, patient care strategies, and resource allocation. For engineers and reliability analysts, the proposed model offers significant advantages in predicting failure times, optimizing maintenance schedules, and improving the reliability of mechanical systems. Broader adoption of this model could lead to more informed, data-driven decisions across healthcare, engineering, and related fields, ultimately optimizing outcomes and improving system reliability and patient care.

AUTHOR CONTRIBUTIONS

S. O. Bashiru: Conceptualization, Methodology, Validation, Writing – original draft, Writing – review &

editing. **A. M. Isa:** Supervision, Writing – original draft, Writing – review & editing. **A. A. Khalaf:** Writing – original draft, Analysis, Writing – review & editing. **M. A. Khaleel**: Supervision, Writing – original draft, Writing – review & editing. **K. C. Arum:** Writing – original draft, Writing – Review & editing. **C. L. Anioke:** Writing – original draft, Writing – Review & editing.

REFERENCES

Adepoju, A. A.; S.S. Abdulkadir and D. Jibasen (2023). 'The Type I Half Logistics-Topp-Leone-G Distribution Family: Model, its Properties and Applications', UMYU Scientifica, 2(4), 9–22.

Ahmad, A.; N. Alsadat; M. N. Atchade; S. Q. ul Ain; A. M. Gemeay; M. A. Meraou; E. M. Almetwally; M. M. Hossain; and E. Hussam. (2023). 'New hyperbolic sine-generator with an example of rayleigh distribution: simulation and data analysis in industry', Alexandria Eng. J. 73: 415-426.

Al-Shomrani, A; O. Arif; A. Shawky; S. Hanif and M. Q. Shahbaz. (2016). 'Topp-Leone Family of Distributions: Some Properties and Application', Pakistan Journal of Statistics and Operation Research, 443-451.

Alobaidi, M. H.; Oguntunde, P. E.; and Khaleel, M. A. (2021). 'The Transmuted Topp Leone Flexible Weibull (TTLFW) distribution with applications to reliability and lifetime data', In Journal of Physics: Conference Series, 1879 (2), 1-11.

Atchadé, M. N.; M. J. Bogninou; A. M. Djibril; and M. N'bouké. (2023). 'Topp-Leone Cauchy Family of Distributions with Applications in Industrial Engineering', J Stat Theory Appl 22, 339–365.

Bashiru, S. O.; A. A. Khalaf; A. M. Isa and A. Kaigama. (2024a). 'On modeling of biomedical data with exponentiated Gompertz inverse Rayleigh distribution', Reliability: Theory & Applications, 19(3 (79)), 460-475.

Bashiru, S. O.; A. A. Khalaf and A. M. Isa (2024b). 'Topp-Leone exponentiated Gompertz inverse Rayleigh distribution: properties and applications', Reliability: Theory & Applications, 19(3 (79)), 59-77.

Benchiha, S.; L. P. Sapkota; A. Al Mutairi; V. Kumar; R. H. Khashab; A. M. Gemeay; M. Elgarhy and S. G. Nassr. (2023). 'A New Sine Family of Generalized Distributions: Statistical Inference with Applications', Math. Comput. Appl. 28*, 83*.

Brito, E.; G. M. Cordeiro; H. M. Yousof; M. Alizadeh and G. O. (2017). 'The Topp–Leone odd log-logistic family of distribution', Journal of Statistical Computation and Simulation, 87(15), 3040-3058.

Cordeiro, G. M.; A. E. Gomes; C. Q. da-Silva and E. M. Ortega. (2013). 'The beta Exponentiated Weibull distribution', Journal of statistical computation and simulation, 83(1), 114-138.

Falgore, J. Y. and Doguwa, S. I. (2020). 'The inverse Lomax-G family with application to breaking strength data', Asian Journal of Probability and Statistics, 8(2): 49–60.

Hassan, A. S. and Assar, S. M. (2017). 'The Exponentiated Weibull power function distribution', Journal of data science, 16(2), 589-614.

Hassan, A. S.; M. Elgarhy and R. Ragab. (2020). 'Statistical properties and estimation of inverted Topp-Leone distribution', J. Stat. Appl. Probab, 9(2), 319-331.

Hosseini, B.; M. Afshari; and M. Alizadeh. (2018). 'The generalized odd gamma-g family of distributions: properties and applications', Austrian J. Stat. 47: 69–89.

Hassan, A. S.; A. W. Shawkia and H. Z. Muhammed. (2022). 'Weighted Weibull-G family of distributions: Theory & application in the analysis of renewable energy sources', *Journal of Positive School Psychology*, 6(3), 9201–9216.

Isa, A. M; S. I. Doguwa; B. B. Alhaji and H. G. Dikko. (2023). 'Sine Type II Topp-Leone G Family of Probability Distribution: Mathematical Properties and Application', Arid Zone Journal of Basic and Applied Research. 2(4): 124 -138.

Khalaf, A. A. and Khaleel, M. A. (2024). 'The New Strange Generalized Rayleigh Family: Characteristics and Applications to COVID-19 Data', Iraqi Journal for Computer Science and Mathematics, 5(3), 92-107.

Khalaf, A. A. M. Q. Ibrahim and N. A. Noori. (2024). '[0, 1] Truncated Exponentiated Exponential Burr type X Distribution with Applications', Iraqi Journal of Science, 4428-4440.

Nanga, S; S. Nasiru and J. Dioggban. (2022). 'Tangent Topp-Leone Family of Distributions', Scientific African, 17, e01363, 1 – 16.

Nanga, S.; S. B. Sayibu; I. D. Angbing; M. Alhassan; A-M. Benson; A. G. Abubakari and S. Nasiru. (2024). 'Secant Kumaraswamy Family of Distributions: Properties, Regression Model, and Applications', Computational and Mathematical Methods, 2024 (1); 1 – 25.

Noor, N. A.; A. A. Khalaf and M. A. Khaleel (2023). 'A New Generalized Family of Odd Lomax-G Distributions Properties and Applications', Advances in the Theory of Nonlinear Analysis and its Applications. 7(4), 01–16.

Oluyede, B.; T. Moakofi; F. Chipepa and B. Makubate. (2020). 'A new power generalized Weibull-G family of distributions: Properties and applications', Journal of Statistical Modelling: Theory and Applications, 1(2), 167-191.

Osi, A. A.; S. I. Doguwa; Y. Abubakar; Y. Zakari and U. Abubakar. (2024). 'Development of exponentiated cosine Topp-Leone generalized family of distributions and its applications to lifetime data', UMYU Scientifica. 2024;3(1):157-67.

Soliman, A. H.; M. A. E. Elgarhy and M. Shakil. (2017). 'Type II half logistic family of distributions with applications', Pak. J. Stat. Oper. Res. 13, 245–264

Souza, L. (2015). 'New trigonometric classes of probabilistic distributions', Estado de Pernambuco - Brasil.

Yousof, H. M.; A. Z. Afify; S. Nadarajah; G. Hamedani and G. R. Aryal. (2018). 'The Marshall-Olkin Generalized-G family of distributions with applications', Statistica, 78(3), 273–295.